atoms

MDPI

Article

Solving Time-Dependent Schödinger Equation for Some PT-Symmetric Quantum Mechanical Problems

Tsin-Fu Jiang

Institute of Physics, National Yang Ming Chiao Tung University, Hsinchu 30010, Taiwan; tfjiang@nycu.edu.tw

Abstract: Using a high-precision code, we generate the eigenstates of a PT-symmetric Hamiltonian. We solve the time-dependent Schrödinger equation (TDSE) of the non-Hermitian system based on the eigenset. Since the formulation is relatively new and the observables are calculated differently than conventional quantum mechanics, we justify it with a paradigmatic case in Hermitian quantum mechanics. We present the harmonic generation spectra on some model PT-Hamiltonians driven by an electric pulse. We discuss the physical differences with the harmonic spectra of a pulse-driven atom.

Keywords: PT symmetry; non-Hermitian quantum mechanics; time-dependent Schrödinger equation

check for updates

Citation: Jiang, T.-F. Solving Time-Dependent Schödinger Equation for Some PT-Symmetric Quantum Mechanical Problems. *Atoms* **2024**, *12*, 46. https://doi.org/10.3390/atoms12090046

Academic Editor: Jean-Christophe Pain

Received: 7 August 2024
Revised: 6 September 2024
Accepted: 9 September 2024
Published: 11 September 2024

Copyright: © 2024 by the author. Licensee MDPI, Basel, Switzerland. This article is an open access article distributed under the terms and conditions of the Creative Commons Attribution (CC BY) license (https://creativecommons.org/licenses/by/4.0/).

1. Introduction

The Hamiltonian is a Hermitian operator in conventional quantum mechanics so that the eigenvalues are all real and the eigenstates are stationary. In 1998, Bender and Boettcher [1] revealed that non-Hermitian Hamiltonians with space-time reflection symmetry and vanishing boundary conditions in Stokes wedges will have real eigenvalues. This parity time reversal was named PT-symmetry, and the Hamiltonian can be complex. Their paper has become highly cited since its inception. A book edited by Bender provides both theoretical and experimental works, updated to 2018 [2]. The related exploration in modern optics has been fascinating [3–6]. Jones reviewed the fundamental theory and many novel experiments in optics in a chapter of Ref. [2]. Consider a medium with variable dielectric function $\epsilon(x)$. The Maxwell equations of $\mathcal{E}$, $\mathcal{H}$ are

$$\nabla^2\mathcal{E} - \mu_0\epsilon(x)\frac{\partial^2}{\partial t^2}\mathcal{E} = \nabla[\epsilon\mathcal{E}\cdot\nabla\frac{1}{\epsilon(x)}], \tag{1}$$

$$\nabla^2\mathcal{H} - \mu_0\epsilon(x)\frac{\partial^2}{\partial t^2}\mathcal{H} = -\frac{1}{\epsilon}\nabla\epsilon(x)\times(\nabla\times\mathcal{H}). \tag{2}$$

For a medium with specific dielectric function in the (x,z)-plane, Burckardt [7] solved the modes of field $\mathcal{E}$ in the polarization plane (E-mode) or in perpendicular to the polarization plane (H-mode). For example , in the E-mode, we can set $\mathcal{H} = \hat{y}H(x,z)e^{ik_0z-i\omega t}$ under the paraxial approximation, (that is, assuming $\frac{\partial^2 H}{\partial z^2} \ll \frac{\partial^2 H}{\partial x^2}$); we then have

$$i\frac{\partial H}{\partial z} = \frac{-1}{2k_0}\{\frac{\partial^2 H}{\partial x^2} + (\omega^2\epsilon\mu - k_0^2)H - \frac{\epsilon(x)'}{\epsilon}\frac{\partial H}{\partial x}\}. \tag{3}$$

The function $H(x,z)$ has a close analogy to the Schrödiner equation with z corresponding to t and the right-hand side corresponding to a stationary eigenvalue Hamiltonian. The electromagnetic wave in the medium has a close analog to the matter wave. We expect that there will be interesting problems to investigate with a complex function $\epsilon(x)$. The PT-symmetric quantum mechanics is then closely related to fundamental physics.

In this paper, we aim to compute the eigenvalue problem of the non-Hermitian Hamiltonian and develop a method to solve the time-dependent Schrödinger equation with an interaction term. We formulate the eigenvalue problem on the Fourier basis. We

use the quadruple precision solver HTDQLS for the complex–symmetric matrix released by Noble et al. [8]. The code calculates eigenvalues and normalized eigenvectors. In a comparison of complex rotated harmonic oscillator ground state energy, the errors of quadruple precision HTDQLS are about 10^{-16} times that of the double precision LAPACK code ZGEEVX [9] at grid numbers around 200 $\sim$ 1000. Our calculation faithfully reproduces some of Bender's tabulated results [10]. Motivated by the development of attosecond science in atomic and molecular physics [11–13], the time-dependent interaction on a PT-Hamiltonian will be interesting. First, we applied the TDSE method for the Hamiltonian $H_0 = -\frac{1}{2}\frac{d^2}{dx^2} + \frac{x^2}{2} + igx^3$ under the dipole interaction term $xf(t)$. With a tiny value of g, the eigenspectrum of H_0 has no visible difference from that of a simple harmonic oscillator. We justify our TDSE algorithm with the paradigmatic example of a driven oscillator [14–16], for which we know the analytical results. Also, we propose the expectation of $(x(t))$ as $(\Psi(x,t)|x|\Psi(x,t))$ in the next section. We calculate the emitted spectrum by taking the Fourier transform of $(x(t))$ [17,18]. We then study several model problems. We interpret the results and explain the fundamental differences from the driven atoms. There are several relevant works on time-dependent problems. Some are in a more general pseudo-Hermitian framework [19–22].

In the rest of the paper, Section 2 presents the method of calculation, Section 3 displays comprehensive results and discussions, and Section 4 includes the concluding remarks. The atomic units are used throughout unless otherwise stated.

2. Method of Calculation

2.1. The Eigenstates

Consider an example PT-symmetric eigenvalue problem in coordinate space,

$$E < x|\psi > \;=\; < x|\frac{-1}{2m}\frac{d^2}{dx^2}|\psi > + < x|V(x)|\psi >, \tag{4}$$

$$V(x) \;=\; \frac{m\omega_0^2}{2}x^2 + igx^3. \tag{5}$$

In the Fourier basis $< x|k >= \frac{1}{\sqrt{2\pi}}e^{ikx}$,

$$\int dk'dx' < x|k' > \frac{-1}{2m}\frac{d^2}{dx^2} < k'|x' > \psi(x') \;=\; \frac{1}{2\pi}\int dk'dx' e^{ik'(x-x')}\frac{k'^2}{2m}\psi(x'), \tag{6}$$

$$< x|V(x)|\psi > \;=\; V(x)\psi(x). \tag{7}$$

Numerically, we use the grids [23]

$$x_k \;=\; k\cdot\Delta x,\; k = -M, -M+1, \cdots, -1, 0, 1, \cdots, M-1, M, \tag{8}$$

$$k_\mu \;=\; \mu\cdot\Delta k,\; \mu = -M, -M+1, \cdots, -1, 0, 1, \cdots, M-1, M, \tag{9}$$

$$\Delta x \;\cdot\; \Delta k = \frac{\pi}{M}. \tag{10}$$

We obtain the matrix eigenvalue equation

$$\frac{1}{M}\sum_{k=-M}^{k=M}\sum_{\mu=1}^{\mu=M}\frac{k_\mu^2}{m}\cos[k_\mu(x_j - x_k)]\psi(x_k) + V(x_j)\psi(x_j) = E\psi(x_j), \tag{11}$$

with the matrix elements

$$H_{j,k} = \frac{1}{M}\sum_{\mu=1}^{\mu=M}\frac{k_\mu^2}{m}\cos[k_\mu(x_j - x_k)] + V(x_j)\delta_{j,k}. \tag{12}$$

This is a complex–symmetric matrix eigenvalue problem within the representation. We use the high-precision code HTDQLS [8] and reproduce the levels we could find for the PT-

symmetric potential. For instance, we obtain precisely the first ten levels of $H = -d^2/dx^2 + ix^3$ listed in Table 1 of [10].

We list the lowest six levels of $H = -d^2/dx^2 + igx^3$ for $g = 0.01, 0.05, 0.1, 0.5$, and 1.0 in Table 1.

Table 1. The lowest six eigenvalues for $H = -d^2/dx^2 + igx^3$ with $g = 0.01, 0.05, 0.1, 0.5$, and 1.0.

g	E_0	E_1	E_2	E_3	E_4	E_5
0.01	0.18326	0.65127	1.19854	1.79321	2.42355	3.08284
0.05	0.34886	1.23979	2.28160	3.41366	4.61360	5.86870
0.1	0.46032	1.63591	3.01059	4.50435	6.08768	7.74379
0.5	0.87629	3.11421	5.73113	8.57473	11.58883	14.74150
1.0	1.15627	4.10923	7.56227	11.31442	15.29155	19.45153

And the lowest six energy levels for $H = -\frac{1}{2m}\frac{d^2}{dx^2} + x^2/2 + igx^3$ with $m = 1$ at a coupling constant g from 10^{-4} to 1 are listed in Table 2.

Table 2. The lowest six eigenvalues for $H = -\frac{1}{2m}\frac{d^2}{dx^2} + \frac{x^2}{2} + igx^3$ with $m = 1, g = 10^{-4}, 10^{-3}, 10^{-2}$, 0.05, 0.1, 0.5, and 1.0.

g	E_0	E_1	E_2	E_3	E_4	E_5
10^{-4}	0.50000	1.50000	2.50000	3.50000	4.50000	5.50000
10^{-3}	0.50000	1.50000	2.50002	3.50005	4.50008	5.50011
10^{-2}	0.50014	1.50088	2.50238	3.50462	4.50760	5.51131
0.05	0.50335	1.52118	2.55564	3.60558	4.67002	5.74811
0.1	0.51254	1.57560	2.68971	3.84603	5.03863	6.26325
0.5	0.64588	2.18448	3.94769	5.85246	7.86517	9.96627
1.0	0.79734	2.77352	5.06782	7.55590	10.19040	12.94420

Since the characteristic polynomials of the matrix representation of the H and its transpose H^t are identical, they have the same set of eigenvalues, but may have different eigenvectors. Let

$$H|u_j >= E_j|u_j >,\ H^t|v_k >= E_k|v_k >, \tag{13}$$

take transpose, and with $H^t = H$ for the complex–symmetric matrix, we then can derive

$$< v_k|H = E_k < v_k|, \tag{14}$$
$$< v_k|\{H|u_j >\} = E_j < v_k|u_j >, \tag{15}$$
$$\{< v_k|H\}|u_j > = E_k < v_k|u_j >, \text{thus} \tag{16}$$
$$< v_k|u_j > = 0, \text{for}\, k \neq j. \tag{17}$$

But, $< v_k|$ is simply the transpose of $|v_k >$ without taking a complex conjugate; we will have the convention of the inner product except for the Hermitian quantum mechanics. We designate the inner product as

$$(v_k|u_j) \equiv \int v_k(x)u_j(x)dx. \tag{18}$$

The convention of the inner product is consistent with the definition on page 87 of Ref. [2], where the inner product associated with a PT-symmetric Hamiltonian is shown as

$$(\psi|\phi) \equiv \int_C dx[\psi(x)]^{PT}\phi(x), \tag{19}$$

where C is a contour that terminates in the Stokes sectors with imposed boundary conditions. So, for an observable, we may define the expectation of $\hat{O}$ as

$$(\psi(x,t)|\hat{O}|\psi(x,t)) \equiv \int dx[\psi(x,t)]^{PT}\hat{O}\psi(x,t). \tag{20}$$

2.2. Time-Dependent Schrödinger Equation, TDSE

Consider that the motion of a charge in a PT-symmetric potential $V(x)$ interacts with an electric field pulse,

$$\mathcal{E}(t) = \mathcal{E}_m \cos^2(\frac{\pi t}{\tau})\sin(\omega t),\ t \in [-\tau/2, \tau/2]. \tag{21}$$

Let

$$H_0 = -\frac{1}{2m}\frac{d^2}{dx^2} + V(x), \tag{22}$$

$$H_0|\varphi_j(x)> = E_j|\varphi_j(x)>, \tag{23}$$

$$H = H_0 + x\mathcal{E}(t), \tag{24}$$

where $\mathcal{E}_m$ is the peak field in atomic units and $\mathcal{E}_m = 1$ corresponds to the peak intensity of 7.02×10^{16} watt/cm^2. τ is the pulse duration and ω is the carrier frequency. The pulse frequency peaked at ω and banded around $(\omega - \Omega,\ \omega + \Omega)$, where $\Omega = 2\pi/\tau$ comes from the pulse shape. For the TDSE,

$$i\frac{\partial\psi(x,t)}{\partial t} = \{H_0 + x\mathcal{E}(t)\}\psi(x,t), \tag{25}$$

$$\psi(x,t) \equiv \sum_j c_j(t)|\varphi_j(x)> e^{-iE_j(t+\tau/2)}, \tag{26}$$

$$i\frac{dc_j(t)}{dt} = \mathcal{E}(t)\sum_k c_k(t)e^{i(E_j-E_k)(t+\tau/2)}(\varphi_j(x)|x|\varphi_k(x)), \tag{27}$$

where the inner product (18) is applied. Let

$$c_j(t) \equiv u_j(t) + iv_j(t), \tag{28}$$

$$(\varphi_j(x)|x|\varphi_k(x)) \equiv x_{j,k} + iy_{j,k}, \tag{29}$$

$$w_{jk} \equiv E_j - E_k,\ t' = t + \tau/2, \tag{30}$$

we then derive

$$\begin{aligned}\frac{du_j(t)}{dt} &= \mathcal{E}(t)\sum_k\{x_{jk}[u_k(t)\sin(w_{jk}t') + v_k(t)\cos(w_{jk}t')] \\ &- y_{j,k}[v_k(t)\sin(w_{jk}t') - u_k(t)\cos(w_{jk}t')]\},\end{aligned} \tag{31}$$

$$\begin{aligned}\frac{dv_j(t)}{dt} &= \mathcal{E}(t)\sum_k\{x_{jk}[v_k(t)\sin(w_{jk}t') - u_k(t)\cos(w_{jk}t')] \\ &+ y_{j,k}[u_k(t)\sin(w_{jk}t') + v_k(t)\cos(w_{jk}t')]\}.\end{aligned} \tag{32}$$

Solving the TDSE becomes the integration of a set of coupled ordinary differential equations with given initial conditions. We use the routine `D02CJF` of NAG [24] which integrates the system by a variable-order, variable-step Adams method.

For the dipole function, we have

$$(\Psi(t)|x|\Psi(t)) = \sum_{j,k} c_j^*(t)c_k(t)e^{i(E_j-E_k)(t+\tau/2)} \int \varphi_j(x)x\varphi_k(x)dx, \quad (33)$$

$$= \sum_{j,k} c_j^*(t)c_k(t)e^{i(E_j-E_k)(t+\tau/2)}[x_{j,k} + iy_{j,k}], \quad (34)$$

$$\equiv (x(t)). \quad (35)$$

The Fourier transformation of the time sequence $(x(t))$ will be related to the emitted harmonic spectrum intensity I [17,18]:

$$I(\omega') = |\frac{1}{\tau}\int_{-\tau/2}^{\tau/2} e^{-i\omega' t}(x(t))dt\,|^2. \quad (36)$$

2.3. Driven Harmonic Oscillator

Consider especially an electron in a harmonic potential driven by electric field $f(t)$, the Hamiltonian in the dipole approximation is

$$H = \frac{-\hbar^2}{2m}\frac{\partial^2}{\partial x^2} + \frac{1}{2}m\omega_0^2 x^2 + xf(t). \quad (37)$$

The transition probability Pb_n from ground state $n = 0$ to state n at large time is given by the Poisson distribution [14–16]:

$$\sigma = \frac{1}{2\hbar m\omega_0}|\int_{-\infty}^{\infty} f(t)e^{i\omega_0 t}|^2, \quad (38)$$

$$Pb_n = e^{-\sigma}\frac{\sigma^n}{n!}, \quad (39)$$

where $\hbar = m_e = \omega_0 = 1$ in the scaled unit. Furthermore, the eigenvalues are $\varepsilon_n = n + 1/2, n = 0, 1, 2\cdots$. We can calculate the dipole function in the Hermitian quantum mechanics as follows:

$$< x(t) >= \int \psi(x,t)^* x\psi(x,t)dx. \quad (40)$$

The Fourier transform of the sequence $< x(t) >$ gives the emitted spectrum. Sakurai listed that the only nonvanishing dipole matrix elements are [25]

$$< n-1|x|n > = \sqrt{\frac{\hbar}{2m\omega_0}}\sqrt{n}, \quad (41)$$

$$< n+1|x|n > = \sqrt{\frac{\hbar}{2m\omega_0}}\sqrt{n+1}. \quad (42)$$

These transition elements are the nearest neighboring states. For a simple harmonic oscillator, all energy levels are equally spaced. Hence, the emitted harmonic will be only one unit of natural frequency. The harmonic mission of a driven simple harmonic oscillator is drastically different from the atomic cases. Applying a laser pulse on an atom will drive the electron back and forth around the parent nucleus. The recollision of the electron wave packet with the nucleus will induce the emission of harmonics [26]. Since the inception of high-order harmonic generations (HHGs), there has been tremendous progress in producing frontier light pulses. The harmonic generation reveals the new field of attosecond physics [11–13]. We will investigate the pulse effects on a PT-symmetric potential. The simple harmonic oscillator will calibrate in the case of a small coupling constant g. As we see in Table 2, the energy levels of case $g = 10^{-4}$ are nearly identical to a simple harmonic oscillator. As an example, the dipole interaction Hamiltonian $H' = x\mathcal{E}(t), t \in (-\tau/2, \tau/2)$ with $\mathcal{E}(t)$ in (21) is a PT-symmetric term. Figure 1a shows the

electric field pulse, and Figure 1b depicts the corresponding frequency spectrum. The pulse frequency peaks at the carrier frequency ω and is banded around a width of the shape frequency Ω.

Figure 2 depicts the excitation from the initial ground state to other states. It is precisely Poisson's distribution (39). Also shown in Figure 2 is the excitation from the ground state of $H_0 = \frac{-1}{2}\frac{\partial^2}{\partial x^2} + \frac{1}{2}x^2 + igx^3$ with $g = 0.0001$. The difference from the exact results of a driven simple harmonic oscillator is negligible, while we calculate the latter by the non-Hermitian TDSE.

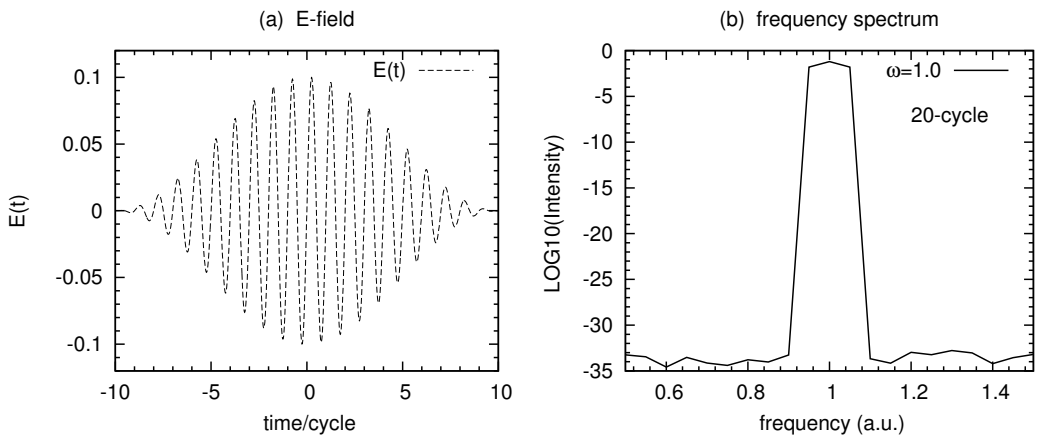

Figure 1. (**a**) The electric field pulse with $\mathcal{E}_m = 0.1, \omega = 1.0, \tau = 20$-cycle. (**b**) The corresponding frequency spectrum of the pulse peaked at ω and banded around $\omega - \Omega$ and $\omega + \Omega$, where ω is the carrier frequency and Ω comes from the pulse duration.

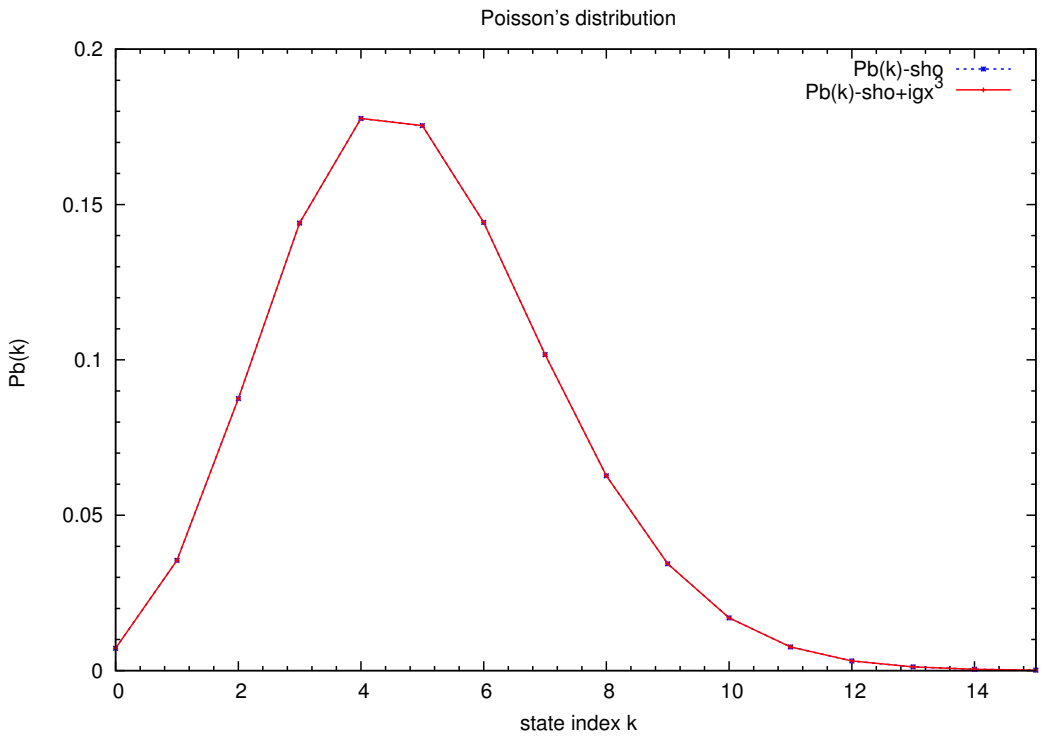

Figure 2. Occupation probability in excited state k after the same pulse of Figure 1 with the initial state in the ground state. The Hermitian quantum mechanical (blue-dotted) results and non-Hermitian one with a small value of $g = 0.0001$ (red) show negligible differences. The connected line is for visual guidance.

3. Results and Discussions

We apply the TDSE method described to study a model PT-system under the dipole interaction $x\mathcal{E}(t)$. The electric field is in the form of (21) with $\mathcal{E}_m = 0.1, \omega = E_1 - E_0, \tau = 20$-cycle, where cycle$= 2\pi/\omega$ for the case in Section 3.1 below, but $\tau = 50$-cycle for the cases in Sections 3.2 and 3.3.

3.1. $H = -\frac{1}{2}\frac{d^2}{dx^2} + \frac{x^2}{2} + igx^3 + x\mathcal{E}(t),\ g = 0.0001$

Table 2 shows that the energy levels without the interacting Hamiltonian $x\mathcal{E}(t)$ are nearly identical to the harmonic oscillator at $g = 0.0001$. Figure 2 shows that the TDSE results of the current case are equal to the Hermitian quantum mechanical Poisson's distribution results of the driving harmonic oscillator. Figure 3a depicts the emitted light from the Fourier transform of $< x(t) >$ (40) of the driven harmonic oscillator and from $(x(t))$ (35) of the non-Hermitian TDSE. The two spectra are nearly identical. It is worth noting that only the natural frequency ω is dominant in these spectra. As the selection rules shown in (42), the only nonvanishing transitions are between the nearest states with the energy difference always equal to ω in both the harmonic oscillator and the PT-system with a minimal value of g. Excitation with resonant frequency will be more efficient than nonresonant excitation. Figure 3b shows the time history of the expansion coefficients (26). The transition from the ground state c_0 to the first excited state c_1 occurs around $t \sim -6.5\tau$, then c_2 starts near $t \sim -4\tau$ and so on. At the end of pulse $t = 10\tau$, the Poisson's distribution is equal to the results shown in Figure 2. We can conclude that the non-Hermitian TDSE formalism and the form $(x(t))$ (35) are correct.

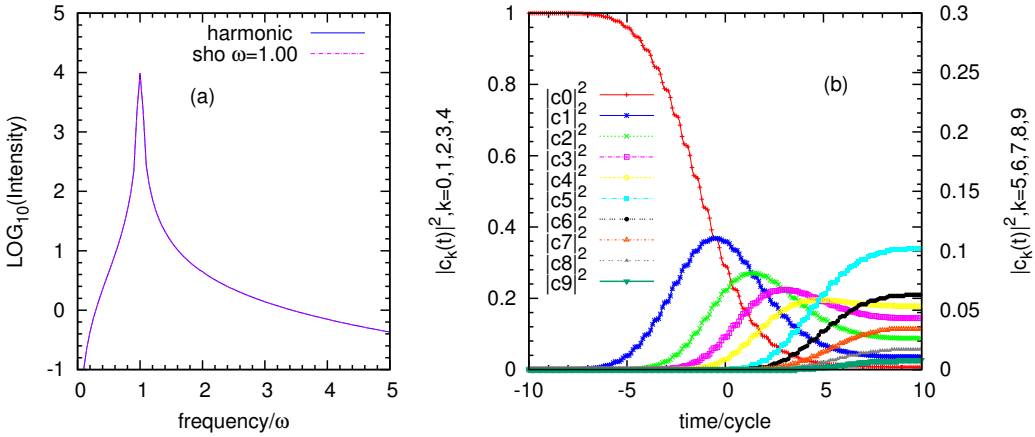

Figure 3. (**a**) The emitted light spectra of a pulse-driven harmonic oscillator. The spectra of a system with an additional term $igx^3, g = 0.0001$ under the same pulse show no difference from those of the harmonic oscillator. (**b**) The time history of dominant coefficients $c_k(t)$ for the pulse-driven harmonic oscillator with an additional term $igx^3, g = 0.0001$. At the end of the pulse, the coefficients are in the Poisson's distribution.

3.2. $H = -d^2/dx^2 + igx^3 + x\mathcal{E}(t),\ g = 0.1\ and\ \ g = 1$

We list the lowest six energy levels for several g-values in Table 1 and the dominant dipole moments in Table 3 for $g = 0.1$ and $g = 1.0$. We can have transitions for quantum number increments in $\Delta n = 1, 2, 3, 4$. Figure 4a plots the emitted light intensity (in logarithmic scale) versus frequency for g = 0.1 at carrier frequency ω resonant to $E_1 - E_0 = 1.1756$. For a 50-cycle duration pulse, we have the frequency band in $(\omega - \Omega,\ \omega + \Omega) = (1.1521,\ 1.1991)$. It characterizes the horizontal frequency positions of the first harmonic. The second harmonic is located at two times of the three frequencies peaked at $2.3042, 2.3512, 2.3982$. The third harmonic is around the frequency in $(3.4563,\ 3.5973)$. In the case of $g = 1$, we use the carrier frequency ω equal to $E_1 - E_0 = 2.9530$. The pulse frequency banded in $(\omega - \Omega,\ \omega + \Omega) = (2.894,\ 3.012)$ and $(2\omega - 2\Omega,\ 2\omega + 2\Omega) = (5.788,\ 6.024)$. Figure 4b shows the emitted frequency spectrum of

the first and second harmonics. In Figure 5, we plot $|(x(t))|$ with time for $g = 0.1$ and $g = 1$. For the interaction-free condition, from the TDSE formulation, we have $dc_j(t)/dt = 0$, and the system will stay with $c_0(t) = 1$. Hence, $(x(t)) = (\psi_0(x, t = 0)|x|\psi_0(x, t = 0))$ is a constant of time. With the dipole interaction, $(x(t))$ oscillates but stays bounded. In the intense pulse-driven atom, the ponderomotive energy of nearly free electrons inside the pulse causes the suppression of photoelectron peaks [27] and the cut-off in HHG [28]. It plays no role in the present cases because the charge motion is bounded.

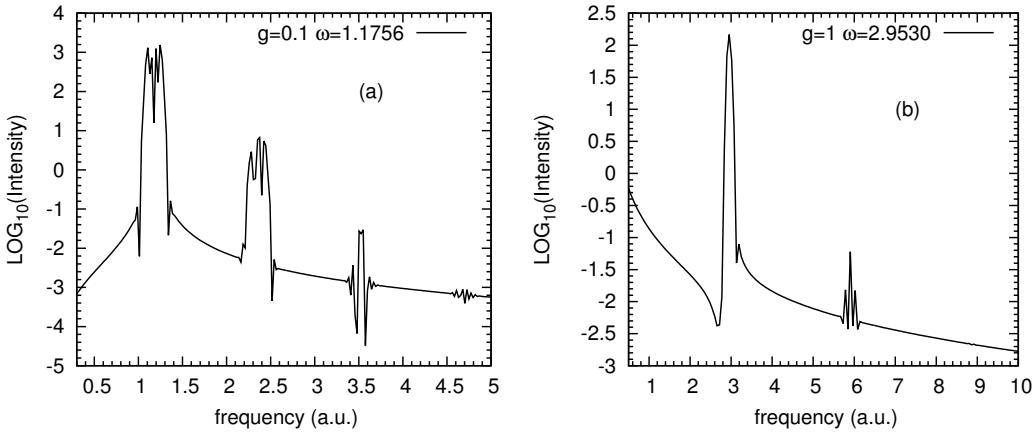

Figure 4. The harmonic generation spectra of Hamiltonian $H = -d^2/dx^2 + igx^3 + xE(t)$ with carrier frequency $\omega = E_1 - E_0$, $\mathcal{E}_m = 0.1$, $\tau = 50$-cycle. (**a**) $g = 0.1$, (**b**) $g = 1$.

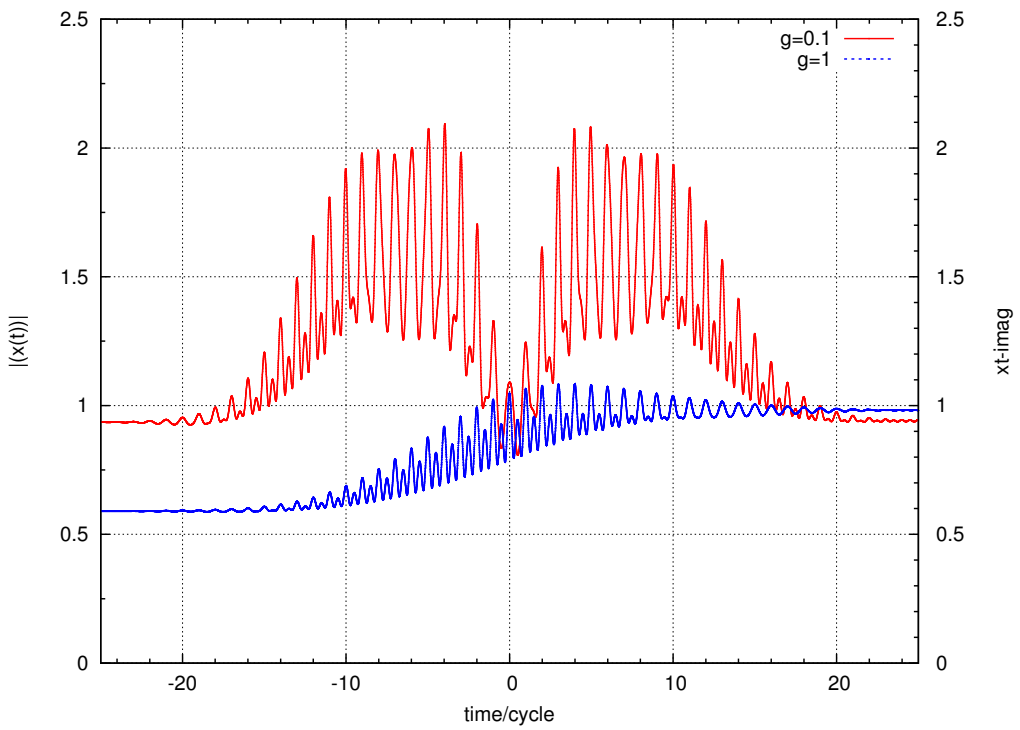

Figure 5. The $|(x(t))|$ versus time of $g = 0.1$ and $g = 1$ for Hamiltonian $H = -d^2/dx^2 + igx^3 + x\mathcal{E}(t)$ with carrier frequency $\omega = E_1 - E_0$, $\mathcal{E}_m = 0.1$, $\tau = 50$-cycle.

Table 3. The matrix elements $(j|x|k)$ for $H = -d^2/dx^2 + igx^3, g = 0.1$ and $g = 1$. Note that $(k|x|j) = (j|x|k)$.

	g = 0.1				g = 1			
j	$(j\|x\|j+1)$	$(j\|x\|j+2)$	$(j\|x\|j+3)$	$(j\|x\|j+4)$	$(j\|x\|j+1)$	$(j\|x\|j+2)$	$(j\|x\|j+3)$	$(j\|x\|j+4)$
0	0.9462	−0.1449 i	−0.0157	0.0015 i	−0.5970	0.0915 i	0.0099	−0.0009 i
1	−1.2486	0.1792 i	0.0188	0.0017 i	−0.7878	0.1131 i	0.0119	−0.0011 i
2	−1.4677	0.2057 i	−0.0213	0.0019 i	−0.9260	0.1298 i	0.0134	−0.0012 i
3	−1.6464	−0.2277 i	−0.0234	0.0021 i	−1.0388	0.1437 i	0.0147	0.0013 i

3.3. $H = -\frac{1}{2}\frac{d^2}{dx^2} + \frac{x^2}{2} + igx^3 + x\mathcal{E}(t)$, $g = 0.1$ *and* $g = 1$

Table 2 shows the lowest six energy levels for several g-values, and Table 4 lists the dominant dipole moments for $g = 0.1$ and $g = 1.0$. The energy levels are generally no longer equally spaced like the harmonic oscillator. The dominant transition moments are for the nearest and following near-neighbor states. Figure 6a depicts the harmonic generation spectrum for $g = 0.1$ driven by the carrier frequency $\omega = E_1 - E_0 = 1.0631$, $\mathcal{E}_m = 0.1$, $\tau = 50$-cycle. The fundamental harmonic has a frequency around $(\omega - \Omega,\ \omega + \Omega)$, where $\Omega = \omega/50$. The frequency is banded in $(2\omega - 2\Omega,\ 2\omega + 2\Omega)$ for the second harmonic. The higher-order harmonics are negligibly small. Figure 6b shows the harmonic spectrum for the case $g = 1$ driven by carrier frequency $\omega = E_1 - E_0 = 1.9762$, $\mathcal{E}_m = 0.1$, $\tau = 50$-cycle. Now that $\Omega = 0.0395$, the fundamental harmonic frequency is in $(1.9367,\ 2.0157)$ and the second harmonic is in $(3.8734,\ 4.0314)$. The higher-order harmonics are negligible unless using a stronger electric field. We display the $|(x(t))|$ versus time in Figure 7. Similar to the previous Section 3.2, the $|(x(t))|$ is bounded and oscillating. Without the field, $(x(t))$ is a constant of time. Again, the ponderomotive energy [27,28] of an ionized electron inside the pulse in a driven atom plays no role here.

Table 4. The matrix elements $(j|x|k)$ for $H = -\frac{1}{2}\frac{d^2}{dx^2} + \frac{x^2}{2} + igx^3, g = 0.1$ and $g = 1$. Note that $(k|x|j) = (j|x|k)$.

	g = 0.1				g = 1			
j	$(j\|x\|j+1)$	$(j\|x\|j+2)$	$(j\|x\|j+3)$	$(j\|x\|j+4)$	$(j\|x\|j+1)$	$(j\|x\|j+2)$	$(j\|x\|j+3)$	$(j\|x\|j+4)$
0	−0.6904	0.0559 i	0.0038	0.0002 i	−0.5154	−0.0770 i	−0.0082	−0.0008 i
1	−0.9585	0.0862 i	−0.0062	−0.0004 i	0.6825	−0.0964 i	0.0100	0.0009 i
2	−1.1560	−0.1108 i	0.0083	0.0006 i	−0.8033	−0.1112 i	0.0114	0.0010 i
3	1.3175	0.1319 i	−0.0102	−0.0007 i	0.9018	0.1235 i	−0.0126	0.0011 i

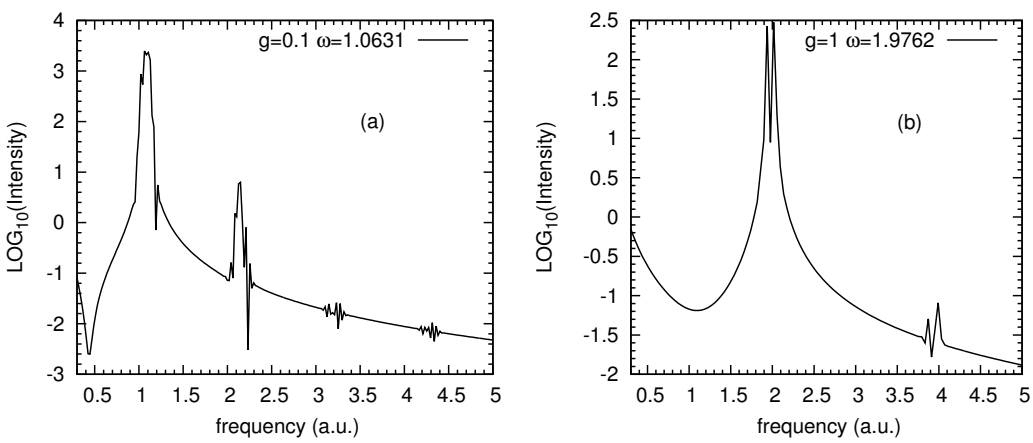

Figure 6. The harmonic generation spectra of Hamiltonian $H = -\frac{1}{2}\frac{d^2}{dx^2} + \frac{x^2}{2} + igx^3 + x\mathcal{E}(t)$ with carrier frequency $\omega = E_1 - E_0$, $\mathcal{E}_m = 0.1$, $\tau = 50$-cycle. (**a**) $g = 0.1$, (**b**) $g = 1$.

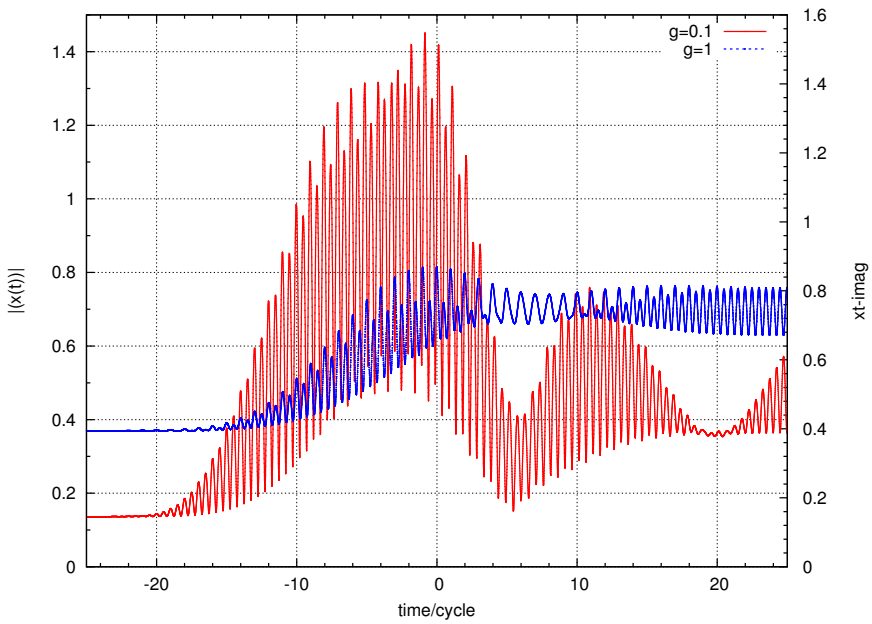

Figure 7. The $|(x(t))|$ versus time of $g = 0.1$ and $g = 1$ for Hamiltonian $H = -\frac{1}{2}\frac{d^2}{dx^2} + \frac{x^2}{2} + igx^3 + x\mathcal{E}(t)$ with carrier frequency $\omega = E_1 - E_0$, $\mathcal{E}_m = 0.1$, $\tau = 50$-cycle.

4. Conclusions

Using the high-precision code HTDQLS [8], we generate the eigenstates of a PT-symmetric Hamiltonian and calibrate the literature results well. The constructed eigenstates are applied to solve the non-Hermitian TDSE. We establish the calculation of observables in non-Hermitian quantum mechanics and justify the method by comparing a pulse-driven harmonic oscillator in Hermitian quantum mechanics and a harmonic oscillator with an additional term igx^3 at $g = 0.0001$. We studied four cases of a PT-Hamiltonian driven by an electric field pulse in dipole approximation in Sections 3.2 and 3.3. The emitted spectra from the Fourier transform of $(x(t))$ show harmonics generated at multiples of the carried frequency with widths of the shape frequency. The nonvanishing transition moments among several nearby states allow the emission of multiple photons. In the case of a harmonic oscillator, there are transition moments between the nearest neighbors only and the energy level difference is ω. Hence, the harmonic spectrum contains simply one photon.

In the atomic high-order harmonic generation, the electric field drives the wavepacket back and forth. The wavepacket collides with the atomic ion twice per cycle; hence, the emitted photon energy spectrum is in 2ω. When the electron is nearly free, the ponderomotive energy is essential. The PT-system we studied has no scattering center and generates different emitted spectra. The ponderomotive energy [27,28] again plays no role in the PT-symmetric cases studied in the paper because the $(x(t))$ is bounded instead of nearly free.

Considering the exponential growth of works in quantum optics with the PT-symmetric model, the investigation by TDSE presented in this paper would be fascinating.

Funding: This research received no external funding.

Data Availability Statement: The data in tables and plots are available from the author upon reasonable request.

Acknowledgments: The author thanks helpful discussions with Chyi-Lung Lin. Expertise comments from the anonymous Referees are gratefully acknowledged.

Conflicts of Interest: The author has no conflicts to disclose.

References

1. Bender, C.M.; Boettcher, S. Real Spectra in Non-Hermitian Hamiltonians Having PT Symmetry. *Phys. Rev. Lett.* **1998**, *80*, 5243–5246. [CrossRef]
2. Bender, C.M. *PT Symmetry in Quantum and Classical Physics*; World Science: London, UK, 2019.
3. El-Ganainy, R.; Makris, K.; Christodoulides, D.; Musslimani, Z. Theory of coupled optical PT-symmetric structures. *Opt. Lett.* **2007**, *32*, 2632–2634. [CrossRef] [PubMed]
4. Zyablovsky, A.A.; Vinogradov, A.P.; Dorofeenko, A.V.; Pukhov, A.A.; Lisyansky, A.A. Causality and phase transitions in PT-symmetric optical systems. *Phys. Rev. A* **2014**, *89*, 033808. [CrossRef]
5. Makris, K.; El-Ganainy, R.; Christodoulides, D.; Musslimani, Z. Beam Dynamics in PT-Symmetric Optical Lattices. *Phys. Rev. Lett.* **2008**, *100*, 103904. [CrossRef] [PubMed]
6. Graefe, E.M.; Jones, H.F. PT-symmetric sinusoidal optical lattices at the symmetry-breaking threshold. *Phys. Rev. A* **2011**, *84*, 013818. [CrossRef]
7. Burckhardt, C.B. Diffraction of a plane wave at a sinusoidally stratified dilectric grating. *J. Opt. Soc. Am.* **1966**, *56*, 1502–1509. [CrossRef]
8. Noble, J.H.; Lubasch, M.; Stevens, J.; Jentschura, U.D. Diagonalization of complex symmetric matrices: Generalized Householder reflections, iterative deflation and implicit shifts. *Comp. Phys. Commun.* **2017**, *221*, 304–316. [CrossRef]
9. Anderson, E.; Bai, Z.; Bischof, C.; Blackford, S.; Demmel, J.; Dongarra, J.; Du Croz, J.; Greenbaum, A.; Hammarling, S.; McKenney, A.; et al. *LAPACK Users' Guide*, 3rd ed.; Society for Industrial and Applied Mathematics: Philadelphia, PA, USA, 1999.
10. Bender, C.M. Making sense of non-Hermitian Hamiltonians. *Rep. Prog. Phys.* **2007**, *70*, 947–1018. [CrossRef]
11. Brabec, T.; Krausz, F. Intense few-cycle laser fields: Frontiers of nonlinear optics. *Rev. Mod. Phys.* **2000**, *72*, 545–591. [CrossRef]
12. Krausz, F.; Ivanov, M. Attosecond physics. *Rev. Mod. Phys.* **2009**, *81*, 163–234. [CrossRef]
13. Lin, C.D.; Le, A.T.; Jin, C.; Wei, H. *Attosecond and Strong-Field Physics*; Cambridge University Press: New York, NY, USA, 2018; Section 5.2.2.
14. Cohen-Tannoudji, C.; Dupont-Roc, J.; Fabre, C.; Grynberg, G. Comment on the Momentum-Translation Approximation. *Phys. Rev. A* **1973**, *8*, 2747–2751. [CrossRef]
15. Ter Haar, D. (Ed.) *Problems in Quantum Mechanics*, 3rd ed.; Chapman and Hall: New York, NY, USA, 1975; Problem 3.41.
16. Jiang, T.F. High-frequency stabilization and high-order harmonic generation of an excited Morse oscillator under Intense Fields. *Phys. Rev. A* **1993**, *48*, 3995–3998. [CrossRef] [PubMed]
17. Lewenstein, M.; Balcou, P.; Ivanov, M.Y.; L'Huillier, A.; Corkum, P.B. Theory of high-harmonic generation by low-frequency laser fields. *Phys. Rev. A* **1994**, *49*, 2117–2132. [CrossRef] [PubMed]
18. Jiang, T.F.; Chu, S.I. High-order harmonic generation in atomic hydrogen at 248 nm: Dipole-moment versus acceleration spectrum. *Phys. Rev. A* **1992**, *46*, 7322–7324. [CrossRef] [PubMed]
19. Jentschura, U.D.; Surzhykov, A.; Lubasch, M.; Zinn-Justin, J. Structure, time propagation and dissipative terms for resonances. *J. Phys. A Math. Theor.* **2008**, *41*, 095302. [CrossRef]
20. Mostafazadeh, A. Consistent Treatment of Quantum Systems with a Time-Dependent Hilbert Space. *Entropy* **2024**, *26*, 314. [CrossRef]
21. Mostafazadeh, A. Pseudo-Hermitian representation of quantum mechanics. *Int. J. Geom. Methods Mod. Phys.* **2010**, *7*, 1191. [CrossRef]
22. Matzkin, A. Non-Hermitian quantum mechanics: The case of bound state scattering theory. *J. Phys. A Math. Gen.* **2006**, *39*, 10859. [CrossRef]
23. Press, W.H.; Teukolsky, S.A.; Vetterling, W.T.; Flannery, B.P. *Numerical Recipes in Fortran*, 2nd ed.; Cambridge University Press: New York, NY, USA, 1992; Chapter 12.
24. *NAG Fortran Library Mark 17*; The Numerical Algorithms Group Inc.: Oxford, UK, 1995.
25. Sakurai, J.J. *Modern Quantum Mechanics*, Revised ed.; Addison-Wesley: New York, USA, 1994; Eq.2.3.25.
26. Chen, Z.; Le, A.T.; Morishita, T.; Lin, C.D. Quantitative rescattering theory for laser-induced high-energy plateau photoelectron spectra. *Phys. Rev. A* **2009**, *79*, 033409. [CrossRef]
27. Chu, S.I.; Cooper, J. Threshold shift and above-threshold multiphoton ionization of atomic hydrogen in intense laser fields. *Phys. Rev. A* **1985**, *32*, 2769–2775. [CrossRef]
28. Corkum, P.B. Plasma perspective on strong field multiphoton ionization. *Phys. Rev. Lett.* **1993**, *71*, 1994–1997. [CrossRef] [PubMed]

Disclaimer/Publisher's Note: The statements, opinions and data contained in all publications are solely those of the individual author(s) and contributor(s) and not of MDPI and/or the editor(s). MDPI and/or the editor(s) disclaim responsibility for any injury to people or property resulting from any ideas, methods, instructions or products referred to in the content.